LRP 423/90 December 1990

ION CYCLOTRON MODES IN A LOW DENSITY PLASMA CAVITY. PART II : EXPERIMENT

M.L. Sawley and P.J. Paris

Ion cyclotron modes in a low density plasma cavity. Part II : Experiment

M.L. Sawley * and P.J. Paris

Centre de Recherches en Physique des Plasmas
Association Euratom-Confédération Suisse
Ecole Polytechnique Fédérale de Lausanne
21, Avenue des Bains, 1007 Lausanne, Switzerland

Abstract. Ion cyclotron modes have been excited in a low density, cylindrical plasma cavity using an external inductive antenna. These modes, which have a long parallel wavelength, exhibit a strong electrostatic character and are only weakly coupled to the antenna fields. Comparison is made of the measured wavefields with those predicted by a theory that includes the influence of electron dynamics. It is thus shown that electron Landau damping, as well as the electron inertia, plays an important role in determining the cavity mode structure.

* Present address: IMHEF-EPFL, ME-Ecublens, 1015 Lausanne, Switzerland

1. Introduction

Ion cyclotron waves have been studied extensively in the past due to their application to plasma heating. Early experiments investigated the absorption of ion cyclotron waves when propagated into a magnetic beach region (see, for example, [1] - [6]). The waves were lauched using an inductive antenna [7] whose length, to achieve optimal coupling for the conditions considered, was relatively short. Initial results [3] indicated that a Faraday shield was necessary to eliminate undesired direct electrostatic coupling between the antenna and the plasma. For the high density range ($n_e \geq 2x10^{12} cm^{-3}$), good agreement was found between the experimental results and the theory that neglected electron inertia (that is, assuming $m_e = 0$). However, in the low density range ($2x10^{10} \leq n_e \leq 2x10^{12}$ cm^{-3}) electron inertia was shown [4], [6] to have a dominant influence on the ion cyclotron wave propagation. The observed heating of the ions in this series of experiments was attributed to resonant ion cyclotron damping, and that of the electrons to both electron Landau damping and ion-electron collisions [2]. However, detailed experiments were not undertaken to study the structure of the wavefields, and no attempt was made to develop a theory that included all of these dissipation effects. Thus, direct quantitative comparison of measured ion cyclotron wavefields with theoretical predictions was not possible.

The present paper reports on an experimental investigation of the excitation of ion cyclotron waves in a magnetized plasma of low density ($n_e \leq 10^{12} cm^{-3}$). A neon plasma, containing the two naturally occuring isotopes Ne^{20} and Ne^{22}, was chosen for this investigation. An electromagnetic wavefield was excited in the plasma column by passing an oscillating current through the external antenna. Detailed measurements of the wavefields were made by inserting magnetic probes into the plasma. Using phase-locked techniques, fields of very low amplitude could be detected. The measured wave

characteristics are compared with the predictions of a theory that incorporates not only the effect of electron inertia, but also electron Landau damping and bulk electron drift (see companion paper [8]).

In Section 2, the experimental set-up used to generate the plasma and excite the ion cyclotron wavefields is presented, as well as a description of the various diagnostics employed to measure the characteristics of both the plasma and the wavefields. The results of the experimental investigation are presented in Section 3, while the comparison with the theoretical predictions of [8] is discussed in Section 4.

2. Experimental set-up

2.1 Experimental apparatus and plasma production

The experiments described here were conducted on the Linear Magnetized Plasma (LMP) device [9]. This is a general-purpose plasma device, having a vacuum vessel with an inner diameter of 0.40 m and a total length of 9.2 m (see figure 1). The vacuum vessel is made of stainless steel (AISI 316L) which ensures a ferrous concentration of less than 1% after welding and machining. The vacuum vessel is constructed of a total of nine sections, with T-sections at each end providing the coupling to the pumping stations. The seven sections inserted inside the magnetic field coils are water cooled on their outer surface as well as on the main flanges. A total of 62 ports permit access for diagnostics at 88 different axial and azimuthal positions. This allows the insertion of optical diagnostics, probes and RF antennas, as well as anodes to change the length of the plasma. A base pressure, with all diagnostics and plasma sources installed, of 1×10^{-7} torr is obtained.

For the present set of experiments, the LMP device was used to provide a cylindrical plasma column of length 4.75 m and diameter 5 cm. The plasma was created using a gas discharge between a heated barium oxide coated cathode located at one end of the device and a plate anode located at the other. The uniform ($\leq 0.3\,\%$) axial magnetic field, $B_0 = 3$ kG used for the present study, was created by passing a d.c. current through a water-cooled solenoid surrounding the vacuum vessel. The current was regulated to compensate for long term drifts. This was accomplished by connecting a 40 kW power supply in series with the 200 kW main power supply. The current fluctuation at 300 Hz was measured to be less than 0.01 % because of the large time constant due to high coil inductance ($\approx$ 50 mH). The current in the magnetic field coils was controlled by a microprocessor, in order to maintain the current within ± 1 A of the nominal setting. The measurement of the current was provided by means of a shunt with a precision of 0.1 %. The microprocessor controller also maintained all the security and safety interlocks and permitted the power supplies (200 kW and 40 kW) to operate together. Thermal bi-metal security switches monitored the temperature of the water inlet and outlet of each field coil.

A neon plasma was used in the present experiments, with naturally occuring neon ($\approx$ 90% Ne^{20}, 10% Ne^{22}) providing a suitable two ion species plasma, as analyzed in the companion paper [8]. The filling gas pressure was maintained in the range of 1.5 to 3.5×10^{-4} torr by feedback control of a piezo-electric inlet value. (The results presented in this paper were obtained with $p_0 = 2 \times 10^{-4}$ torr.) A d.c. discharge current was maintained in the range of 0.02 to 6.0 A. This created a plasma of density in the range 10^{10} to 8×10^{11} cm^{-3}, as measured by a 30.6 GHz microwave interferometer located 1 m from the cathode, following the empirical law

$$n_e / p_0 I_{cathode} \approx 3.9 \times 10^{14}\ cm^{-3} / \text{torr amp} \quad .$$

The percentage ionization of the plasma formed was less than 5 %. For the above-mentioned ranges of filling pressure and discharge current, the on-axis electron temperature measured by Langmuir probes situated at various axial locations was in the range $5 \leq T_e \leq 12\,eV$. Typical electron density and temperature profiles shown in figure 2 indicate that these quantities are relatively uniform across the plasma cross-section, although the density has inevitable gradients near the plasma boundary. The electron temperature was measured to vary by less than 50 % along the entire length of the plasma. Although not directly measured, the axial gradient of the electron density is expected to be of the same order as that of the electron temperature. The relative densities of the two ion species were measured using Doppler-free, two photon, laser-induced fluorescence spectroscopy [10]. Within the measurement error, the concentration of the two ions species was determined to be the same as that of the neutral atoms. This is to be expected, due to the close similarity of ionization cross-sections for atoms of the two neon isotopes. The ion temperature was measured by laser-induced fluorescence spectroscopy to be $T_i \leq 0.2\,eV$.

2.2 Wave excitation

The wavefield in the plasma was produced using a Stix coil [7] surrounding the column. This inductive antenna consists of four separate modules, alternately de-phased by 180° (by reversing the direction of current flow) and placed at regular intervals along the machine. Each module is 67.5 cm in length and 12 cm in diameter, while the spacing between the centres of neighbouring modules is 135 cm. Each module consists of 24 turns of square section copper tubing separated into six sub-coils and joined by straight sections. This design was chosen to avoid reducing the diagnostic access to the region beneath the antenna modules, the sub-coils being aligned beneath the main magnetic field coils of the LMP device. The design includes a Faraday shield between the wave coils

and the plasma. The shield was constructed from a copper tube of thickness ≈ 1 mm (at 200 kHz, skin depth ≈ 0.2 mm), with eight equally-spaced axial cuts along almost the entire length [11]. The Faraday shield was observed to be necessary to avoid spurious electrostatic coupling to the plasma due to the inductive voltage drop along the length of each antenna module. Without the Faraday shield there was also observed evidence of arcing along the modules, this being eliminated by the presence of the shield. Each module of the Stix coil was individually water cooled, allowing for steady state operation. The antenna was driven, via a capacitor matching circuit, by a 1 kW solid state amplifier (ENI model 1140 LA, flat gain for 9 kHz < f < 250 kHz). The antenna circuit, including connections and matching circuit, was found to have a resistance of approximately 1.5 Ω. This allowed an oscillating current of maximum amplitude I_{rf} = 50 A to be driven in the antenna. Figure 3 gives a schematic diagram of the antenna and matching circuit construction.

2.3 Wave detection

The magnetic wavefield was detected by pick-up coils positioned at various axial locations along the LMP device. These probes could be moved to yield radial profiles of the wavefield. Each probe was constructed by winding 60 turns of 0.05 mm diameter insulated wire on a mica former of cross-section 0.15 mm x 1.0 mm. The resulting probes were calibrated using a Helmholtz coil. They had an effective area of NA ≈ 8 x 10^{-5} m^2, yielding an unintegrated signal of ≈ 10 mV/gauss for a frequency of 200 kHz. In order to detect low signal levels, a phase-locked detection system was used. The probe output after pre-amplification was fed into a high frequency lock-in (PAR Model 5202). The current in the antenna was used to calibrate the phase of the reference signal. Phase shifts that may have been introduce by the probe, pre-amplifier or cables were corrected for in the lock-in circuitry. The in-phase and quadrature outputs of the lock-in were recorded,

yielding the in-phase and out-of-phase amplitudes of the magnetic wavefield. Figure 3 shows a schematic diagram of the probe detection system.

All the measurements presented here were obtained with a d.c. plasma, although it was possible to use the lock-in system with a pulsed plasma for a pulse length ≥ 5 ms. The probe signals were neither filtered nor integrated. However, since the frequency is fixed by that of the antenna current, and both in-phase and out-of-phase signals are monitored, it is straightforward to deduce the field amplitude and phase.

An attempt was also made, using a capacitive double probe, to measure the electric field of the wave excited in the plasma. While a deal of effort was taken to shield properly the probe shaft from electrostatic pick-up, it was noticed that the probe signals were very sensitive to plasma noise and to the proximity of the antenna modules. Thus meaningful measurements of the electric field in the presence of the plasma could not be obtained.

It should be noted that for the low density plasma considered, the power input to the plasma was not significant: the vast majority of the available 1 kW amplifier power was dissipated in the resistance of the antenna, matching circuit, leads and connections. It was therefore not possible to detect plasma coupling via a change in the antenna impedance.

3. Experimental results

3.1 General observations

A number of qualitative observations can be made from the recorded magnetic probe signals. Beneath the antenna modules, the magnetic wavefield was found to be essentially

axial, that is, it contained essentially only a B_z component. For the maximum antenna current of I_{rf} = 50 A, the axial magnetic wavefield beneath the antenna modules was measured to be B_z = 15.2 gauss. The azimuthal component, B_θ, in the vicinity of the antenna modules was negligible within the measurement limits. For the plasma parameters considered, there was no noticeable change in the B_z measured beneath the antenna modules due to the presence of a plasma.

Between the antenna modules (that is, at an axial distance greater than the decay length of the vacuum field), the magnetic wavefield in the presence of the plasma was essentially azimuthal: the small B_z wavefield detected was at least an order of magnitude smaller. When measuring the B_θ wavefield, a signal was always detected in the absence of a plasma due to the presence of electrical pick-up. The values of B_θ presented in the following section are the difference between signals recorded with and without plasma.

When the probe was rotated through 180°, the amplitude of the signal (with - without plasma) was found to remain essentially unchanged, but the phase changed by 180°. This is an indication that the probe was actually measuring the magnetic wavefield, and not just electrical pick-up. The lock-in system described in Section 2.3 was shown to be capable of measuring very small field amplitudes (resolution $\leq$ 1 mgauss).

3.2 Wave measurements

Since in the absence of plasma, the azimuthal magnetic field is everywhere zero (assuming that the antenna current is purely azimuthal, as ideally imagined), a coupling to the plasma from the antenna can be implied by measuring an azimuthal field in the presence of the plasma. This is most conveniently undertaken at an axial position midway between two antenna modules where this component of the magnetic wavefield should be

a maximum [8]. Figure 4 shows the results of such a measurement, using a probe located midway between the first and second antenna modules, 1 m from the cathode. The probe was positioned at the mid-radius value, r = 1.25 cm. The in-phase component is plotted for four different values of discharge current (and therefore plasma density, since n_e is proportional to $I_{cathode}$) in figure 4(a), and the out-of-phase component in figure 4(b).

From figure 4(a) it can be noticed that there is a resonance in the in-phase component of B_θ in the vicinity of the cyclotron frequency of the majority (Ne^{20}) ion species. The resonance has a full width at half amplitude of $\approx$ 40 kHz. Both the resonance frequency and width appear to be independent of plasma density. No noticeable effect occurs at the cyclotron frequency of the minority (Ne^{22}) species. Figure 4(b) shows that the out-of-phase component of B_θ increases strongly as the frequency passes from below $\omega_c(Ne^{22})$ to above $\omega_c(Ne^{20})$. Again, the form of the curves obtained appears to be independent of plasma density.

That the observed resonance of the azimuthal wavefield B_θ is dependent on the ion cyclotron frequency is demonstrated in figure 5. In this figure is shown the results of similar measurements obtained with a slightly lower value of B_0 = 2.85 kG. (It can be assumed that there is little change in the plasma parameters, e.g., n, T, for this small change in B_0.) The resonance is again observed in the vicinity of the cyclotron frequency of the majority species.

The dependence on plasma density of the in-phase component of B_θ(r = 1.25 cm) for f = 220 kHz is shown in figure 6. For $I_{cathode} \geq 0.5$ A (and the neutral pressure considered), the wavefield amplitude is found to be proportional to the plasma density. An increase of the wavefield amplitude was also measured as the filling gas pressure was increased.

Radial profiles of the in-phase component of B_θ(f = 220 kHz) measured midway between two antenna modules are shown in figure 7. This figure demonstrates that the radial profile of the in-phase component of B_θ is independent of plasma density.

Measurements were also made by exciting only one antenna module (third from cathode) and measuring the signal on magnetic probes situated at various distances (towards the cathode) from the module. The dependences of the in-phase and out-of-phase components of B_θ were found to have the same forms as for the excitation of four modules. In principle, by exciting only one module, it is possible to measure the phase velocity and attenuation length of any waves launched. However, the measurements made could not be interpreted simply in this manner. In fact, there appeared to be present in the plasma a combination of both propagating and standing waves, due presumably to the long damping length (compared to the machine length) of the waves launched. The standing waves could be eliminated by using a short pulse of r.f. current to the antenna module. However, for such excitation, it was not possible to use the sensitive phase-locked detection system: the resultant noise problems rendered useful measurements impossible.

4. Discussion

The wavefields measured using the magnetic probes, as described in the previous section, can be compared to the results of the numerical calculations for ion cyclotron modes presented in the companion paper [8]. It should be borne in mind, however, that the theory developed in [8] assumes that the plasma is uniform, while in the experimental device gradients exist in both the radial and axial directions. A comparison of results thus

necessitates the use of "average" values of the experimental plasma quantities. While the appropriate averaging procedure is not obvious, it appears reasonable to use radially-averaged values measured at the axial position of the magnetic probe location. The values relevant to the experimental results presented in figures 4 - 7 are then $n_e = 7.8 \times 10^{10}$ cm^{-3} / amp, and $T_e \approx 5$ eV (the local electron temperature being measured to depend only weakly on the discharge current).

Firstly, it can be noted that the observation of a magnetic wavefield that is almost entirely axial beneath the antenna modules, and azimuthal midway between modules, is consistent with the theoretical results. The axial component of the magnetic wavefield, for example, exhibits an antinode midway between modules. The fact that the wavefield measured beneath the modules is essentially axial indicates that the coupling between the inductive antenna and the plasma is weak, as confirmed theoretically. Detailed comparison between the measured wavefields and the theoretically predicted ion cyclotron modes is thus best achieved by consideration of the fields midway between antenna modules.

The amplitude of the azimuthal component of the wavefield can theoretically be shown [12] to be approximately given by

$$B_\theta \;\alpha\; \frac{\mathcal{S}}{\omega\, k_{//}}\, J_1(k_{\perp 1} r)\; I_{rf} \quad , \tag{1}$$

where $k_{//}$ and $k_{\perp 1}$ are the values corresponding to the dominant axial mode. For the parameters of the present experiment, $k_{//}$ is independent of n_e, and $\mathcal{S}$ is proportional to n_e. Thus the wavefield amplitude at a given spatial location is proportional to the plasma density, as confirmed by the results presented in figure 6.

bulk electron drift velocity in the plasmas considered for the present investigation is sizeable ($V_{de} \approx 4x10^4$ ms^{-1} / amp), this has been shown to have little effect on the resonant curves [8].

5. Conclusions

The above observations demonstrate that ion cyclotron modes have been excited in a low density magnetized plasma column. Although these modes are essentially electrostatic in character, they are weakly coupled to the inductive antenna employed. Generally good agreement has been obtained between the measured magnetic wavefields and those calculated using theory developed in the companion paper [8]. For the parameters of the present study, the electron dynamics play an important role in determining the wavefields, not only via the electron inertia but also via electron Landau damping. Thus the present investigation shows that it is essential to account for the collisionless damping of the electrons, even for the low frequencies ($\omega \approx \omega_{ci}$) and low temperatures ($T_e \approx 5$ eV) considered.

Acknowledgements

The authors wish to thank the technical groups for their excellent support in the present work. Other members of the LMP group are also acknowledged for their assistance. This work was partially supported by the Fonds National Suisse de la Recherche Scientifique.

The radial profiles of the azimuthal magnetic wavefield are seen from figure 7 to resemble a distorted $J_1(k_{\perp 1}r)$ Bessel function. The distortion, compared to the theoretical dependence given in equation (1) (see also [8]), is presumably the result of density gradients in the vicinity of the plasma edge (see figure 2).

The azimuthal magnetic component of the ion cyclotron mode is calculated in [8] to exhibit a maximum in the in-phase component in the vicinity of the ion cyclotron frequencies, and a change of sign in the out-of-phase component as the frequency is swept through the ion cyclotron range of frequencies. This typical resonance behaviour is also apparent in the measured values presented in figure 4. The full width at half amplitude of the in-phase component is determined both theoretically and experimentally to be $\approx 40\,\text{kHz}$, and insensitive to the plasma density. It is important to note that this resonance width is much larger than is calculated if only collisional damping is assumed to be present [8]. Thus the inclusion of electron Landau damping is shown to account for the measured resonance width.

While the measured resonance width is correctly predicted by the theoretical calculations of [8], a comparison of the experimental results of figure 4 with the theoretical results given in figure 5 of [8] reveals that the peak amplitude of the B_θ wavefield is measured to be significantly less than theoretically predicted. Different sources of origin of this discrepancy can be proposed. Firstly, the measured value of the amplitude of the vacuum B_z wavefield beneath the coil modules is only ≈ 72 % of that theoretically predicted, due presumably to the approximate modelling of the antenna by a purely azimuthal current sheet. Another source that contributes to the discrepancy in amplitude is the theoretical assumption of a uniform plasma. As remarked above, radial non-uniformities in the plasma lead to a distortion of the radial profile of the wavefields, and consequently a decrease in their amplitude at the mid-radius position. It should be noted that although the

References

[1] W.M. Hooke, F.H. Tenney, M.H. Brennan, H.M. Hill and T.H. Stix, *The Physics of Fluids*, **4**, 1131 (1961).

[2] S. Yoshikawa, M.A. Rothman and R.M. Sinclair, *Physical Review Letters*, **14**, 214 (1965).

[3] M.A. Rothman, R.M. Sinclair and S. Yoshikawa, *Plasma Physics*, **8**, 241 (1966).

[4] J.C. Hosea and R.M. Sinclair, *Physical Review Letters*, **23**, 3 (1969).

[5] M.A. Rothman, R.M. Sinclair, I.G. Brown and J.C. Hosea, *The Physics of Fluids*, **12**, 2211 (1969).

[6] J.C. Hosea and R.M. Sinclair, *The Physics of Fluids*, **13**, 701 (1970).

[7] T.H. Stix, *Theory of Plasma Waves*, McGraw-Hill, New York (1962).

[8] M.L. Sawley, companion paper.

[9] M.Q. Tran, P. Kohler, P.J. Paris and M.L. Sawley, Lausanne Report LRP 205/82 (1982).

[10] P. Kohler, "Doppler-free laser spectroscopy of a noble gas plasma", Ph.D. Thesis No. 626 EPF-Lausanne (1986).

[11] N.B. Dodge, M. Kristiansen and A.A. Dougal, *Review of Scientific Instruments* **37**, 1455 (1966).

[12] M.L. Sawley and M.Q. Tran, Lausanne Report LRP 206/82 (1982).

Figure Captions

Figure 1. The Linear Magnetized Plasma (LMP) device.

Figure 2. Typical radial profiles of (a) electron density, and (b) electron temperature, corresponding to $p_0 = 2 \times 10^{-4}$ torr and $I_{cathode} = 1.5$ A.

Figure 3. Schematic diagram of the antenna and matching circuit construction, together with the probe detection system.

Figure 4. Frequency dependence of (a) the in-phase component, and (b) the out-of-phase component of the azimuthal magnetic wavefield $B_\theta(r = 1.25$ cm) measured midway between two antenna modules.

Figure 5. Same as figure 4 for $I_{cathode} = 2$ A, except for a slightly lower value of the steady axial magnetic field, $B_0 = 2.85$ kG.

Figure 6. Dependence on discharge current of the in-phase component of the azimuthal magnetic wavefield $B_\theta(r = 1.25$ cm) measured midway between two antenna modules for f = 220 kHz.

Figure 7. Radial dependence of the in-phase component of the azimuthal magnetic wavefield $B_\theta(f = 220$ kHz) measured midway between two antenna modules.

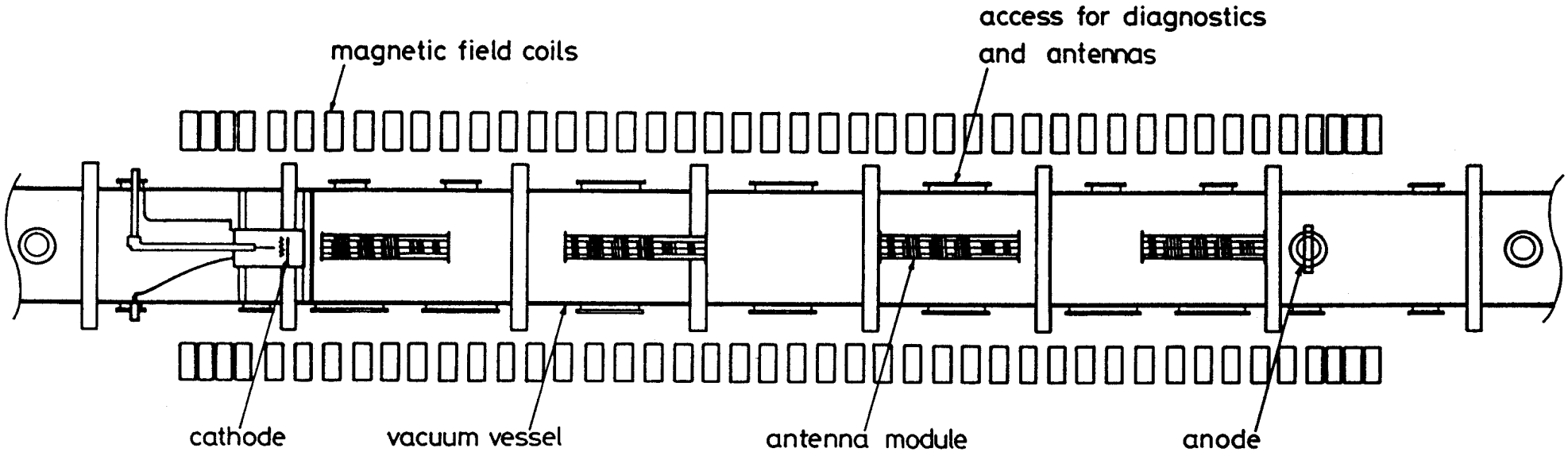
magnetic field coils
access for diagnostics
and antennas
cathode
vacuum vessel
antenna module
anode

Figure 1

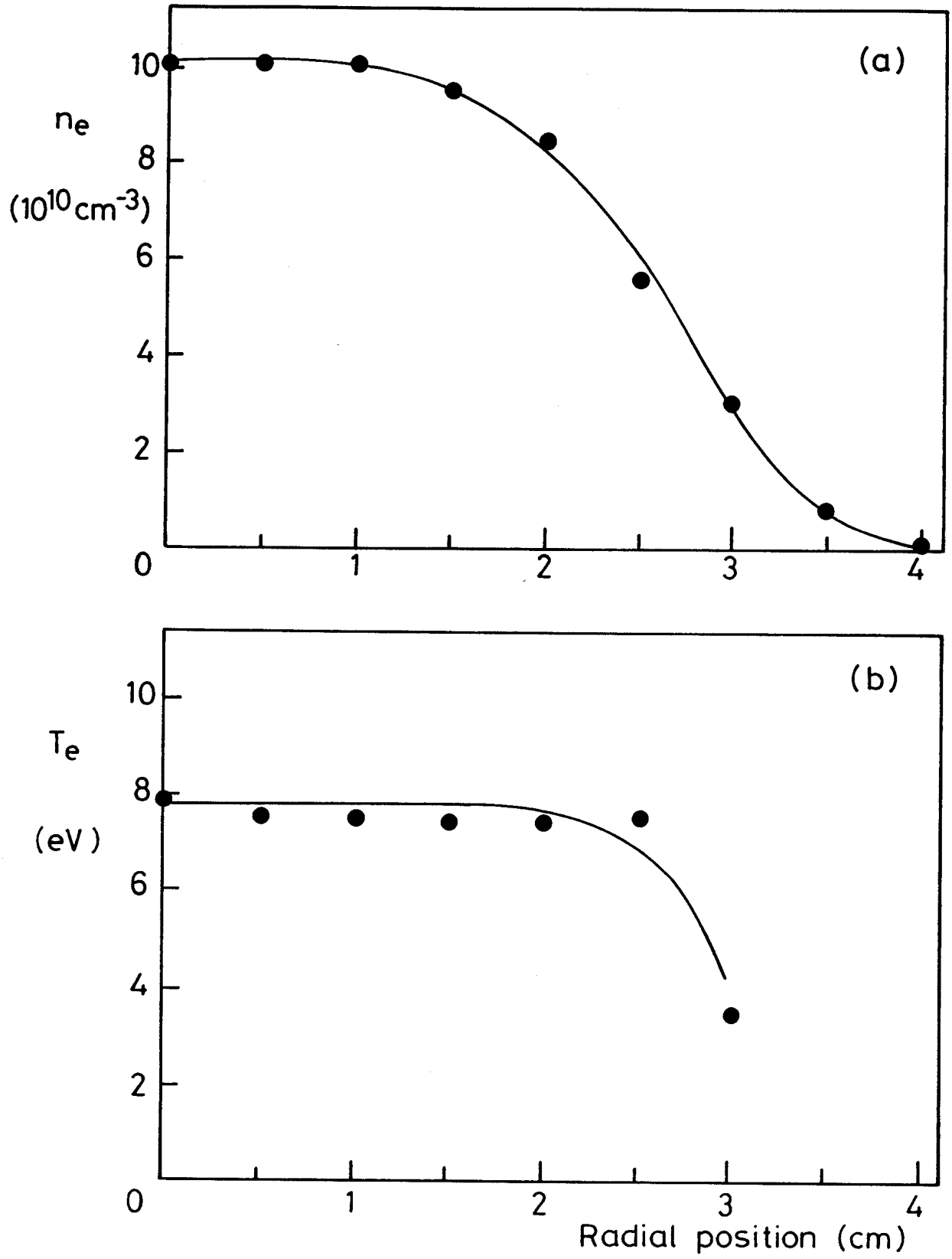
(a)
n_e
$(10^{10} cm^{-3})$
10
8
6
4
2
0
1
2
3
4
(b)
T_e
(eV)
10
8
6
4
2
0
1
2
3
4
Radial position (cm)

Figure 2

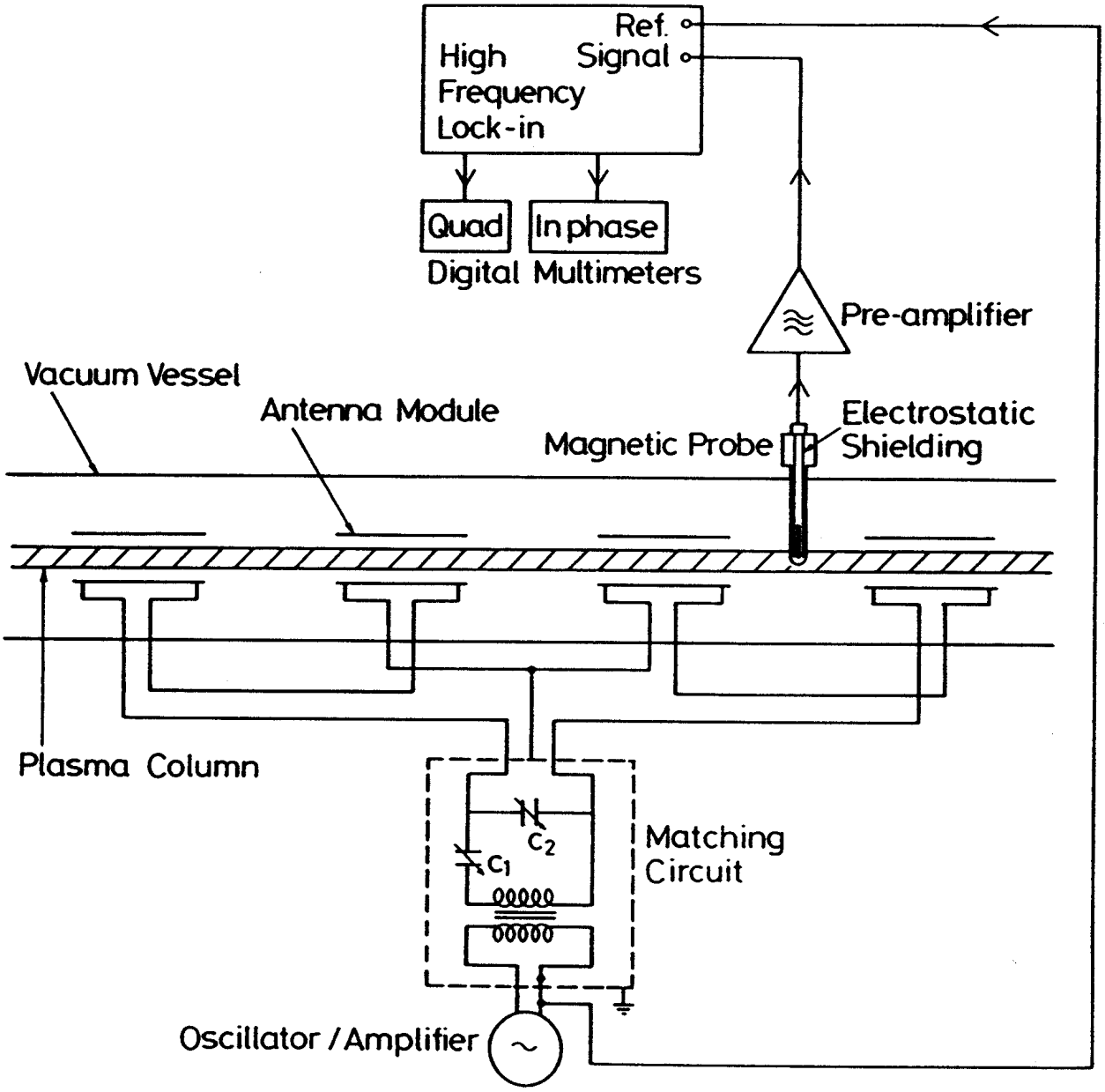
Ref.
High
Frequency
Lock-in
Signal
Quad
In phase
Digital Multimeters
Pre-amplifier
Vacuum Vessel
Antenna Module
Magnetic Probe
Electrostatic
Shielding
Plasma Column
C2
C1
Matching
Circuit
Oscillator / Amplifier

Figure 3

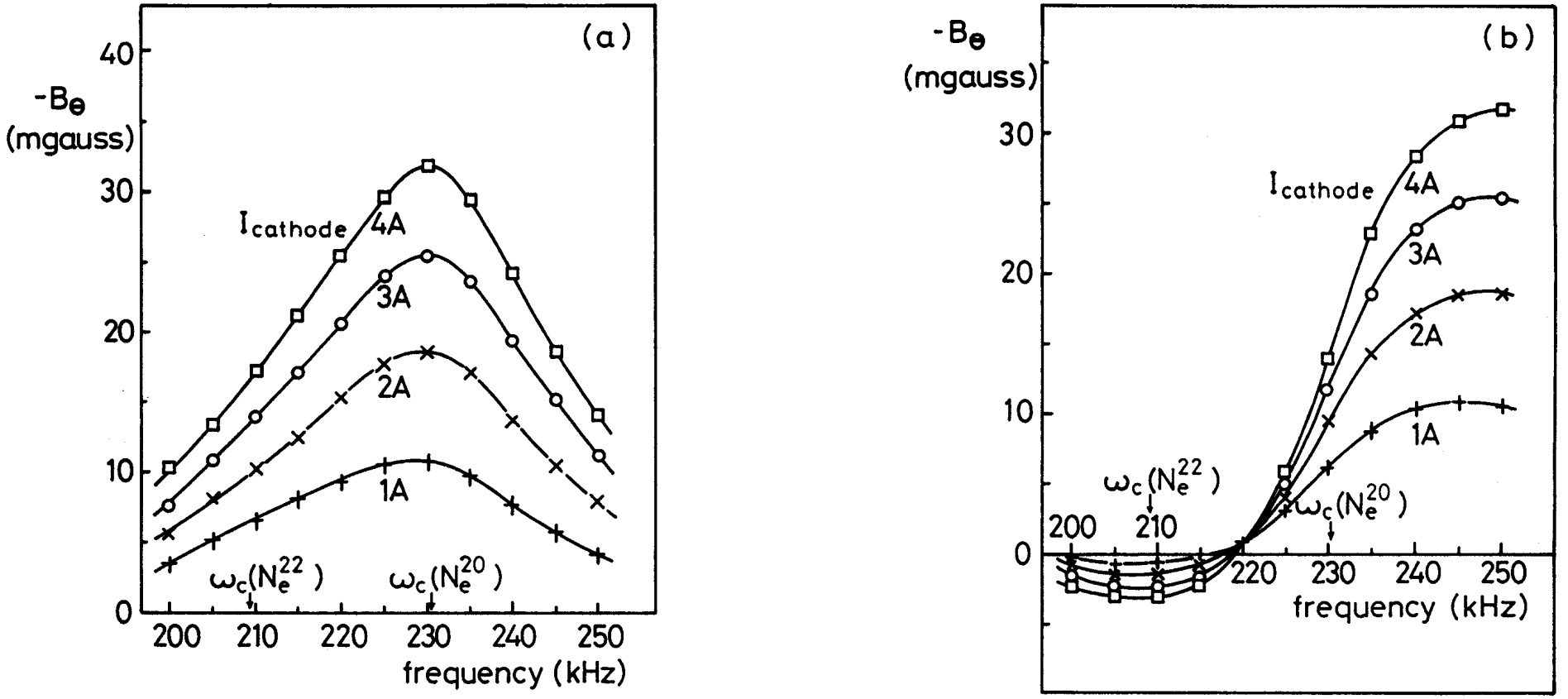
(a)
-Be
(mgauss)
40
30
20
10
0
Icathode
4A
3A
2A
1A
ωc(Ne22)
ωc(Ne20)
200
210
220
230
240
250
frequency (kHz)
(b)
-Be
(mgauss)
30
20
10
0
Icathode
4A
3A
2A
1A
ωc(Ne22)
ωc(Ne20)
200
210
220
230
240
250
frequency (kHz)

Figure 4

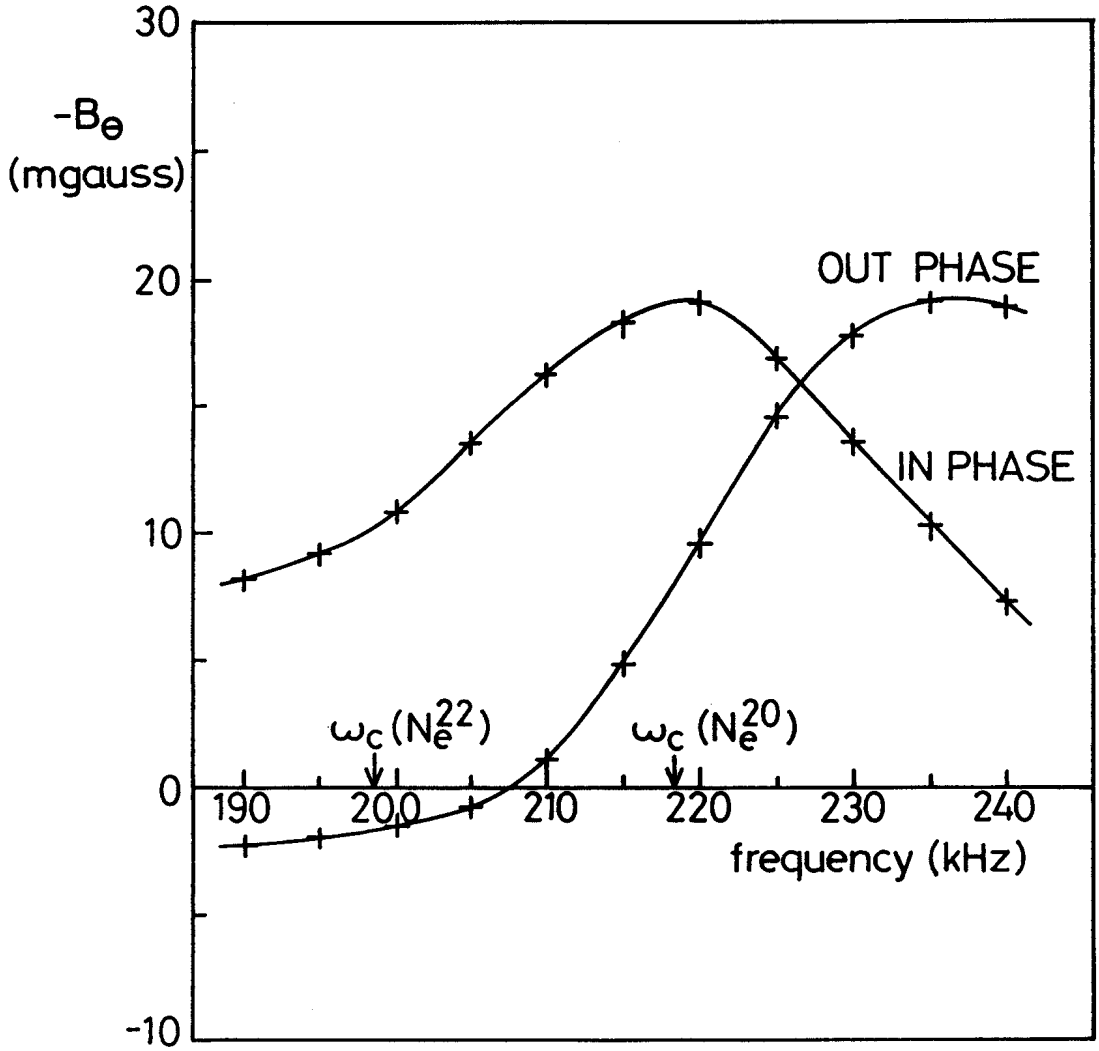
30
-Bθ
(mgauss)
20
10
0
-10
OUT PHASE
IN PHASE
ωc (Ne22)
ωc (Ne20)
190
200
210
220
230
240
frequency (kHz)

Figure 5

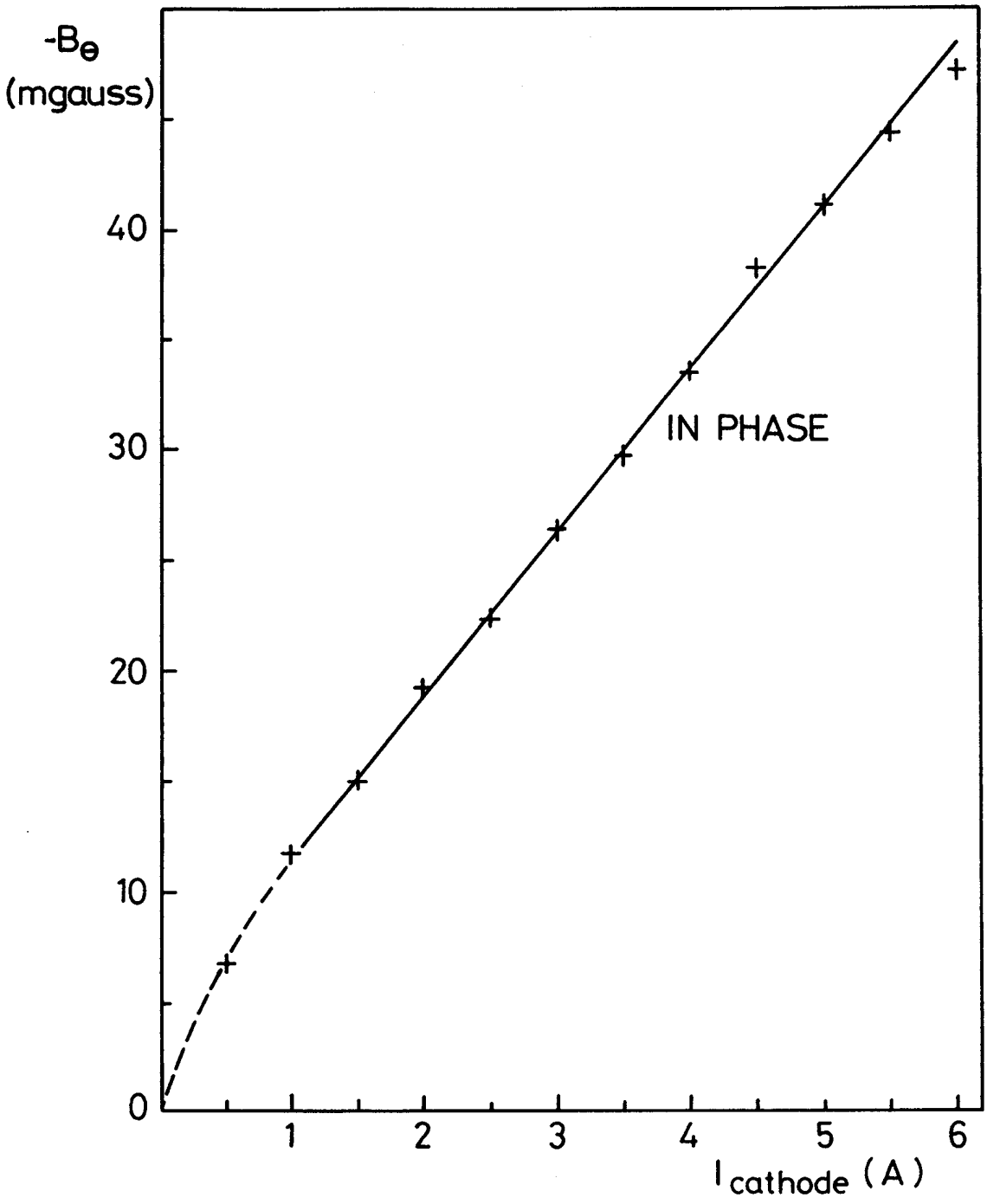

Figure 6

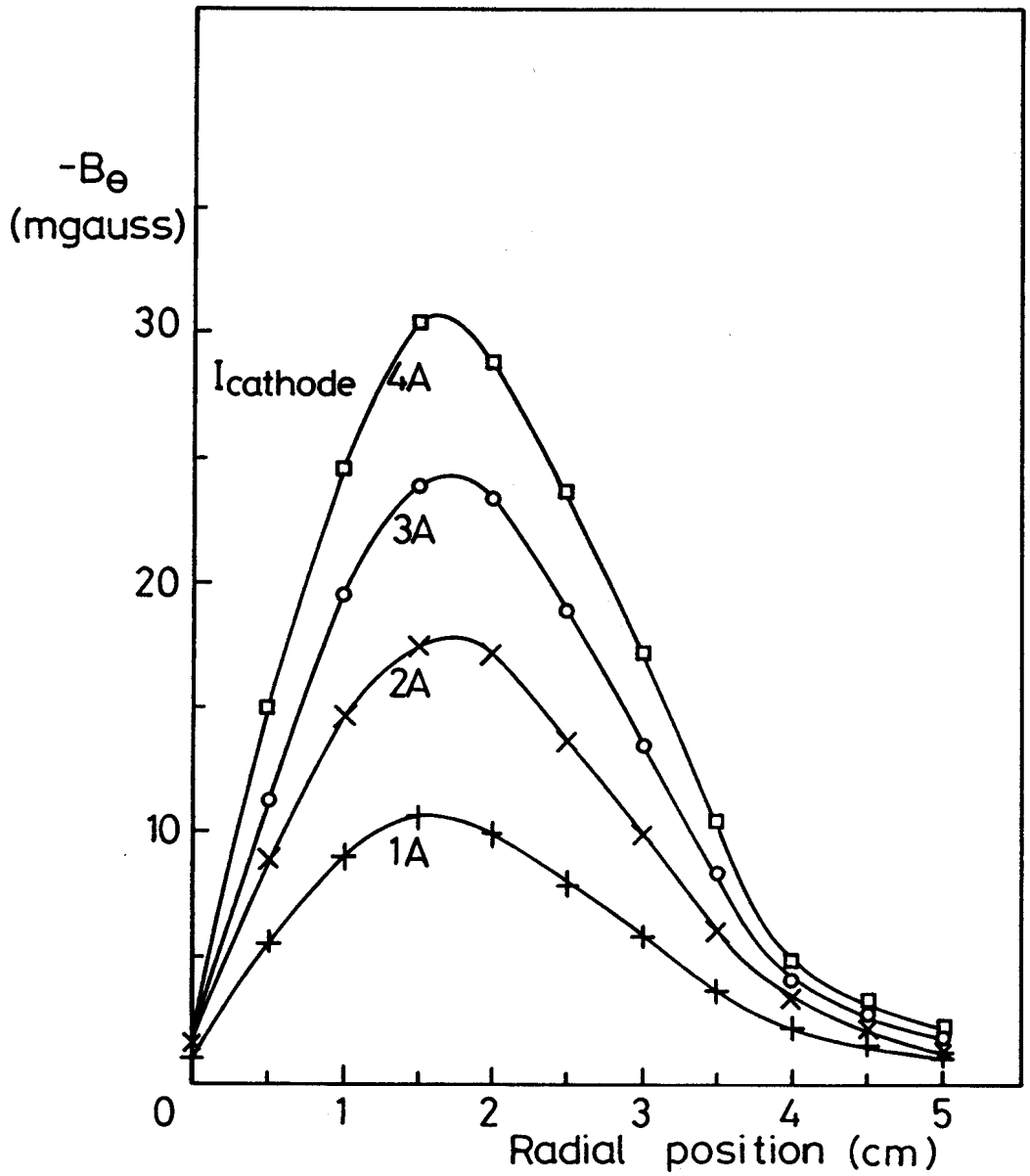
-Bθ
(mgauss)
30
20
10
0
Icathode
4A
3A
2A
1A
1
2
3
4
5
Radial position (cm)

Figure 7